Projected evolution of the Urban climate and heatwaves using an ensemble of convection-permitting regional climate models

Yohanna Michau, A. Lemonsu, P. Lucas-Picher, Sophie Bastin, Cécile Caillaud, H. de Vries, M. Adinolfi, M. Raffa, E. Katragkou, E. Coppola

Projected Evolution of the Urban Climate and Heatwaves using an Ensemble of Convection-Permitting Regional Climate Models

Michau, Y.[1,2,*], Lemonsu, A.[1], Lucas-Picher, P.[1,3], Bastin, S.[4], Caillaud, C.[1], de Vries, H.[5], Adinolfi, M.[6], Raffa, M[6], Katragkou, E.[7] Coppola, E.[8]

[1] CNRM, Université de Toulouse, Météo-France, CNRS, Toulouse, France
[2] Météo-France, Division DSM/CS/DC, Toulouse, France
[3] Département des sciences de la Terre et de l'atmosphère, Université du Québec à Montréal, Montréal, Canada
[4] LATMOS/IPSL, UVSQ Université Paris-Saclay, Sorbonne Universite, CNRS, CNES, Paris, France
[5] Royal Netherlands Meteorological Institute (KNMI), De Bilt, Netherlands
[6] Fondazione Centro Euro-Mediterraneo sui Cambiamenti Climatici, Regional Model and Geo-Hydrological Impacts (REMHI) Division, Via Thomas Alva Edison, 81100, Caserta, Italy
[7] Department of Meteorology and Climatology, School of Geology, Aristotle University of Thessaloniki, Thessaloniki, Greece
[8]International Centre for Theoretical Physics (ICTP), Trieste, Italy

* Corresponding author: yohanna.michau@meteo.fr

Abstract

With climate change, the challenges associated with extreme heat in cities are becoming ever more pressing. There is a need for accurate climate change projections for cities, and for robust quantification of changes in extreme temperatures under the combined effect of global warming and urban heat effect. The present study takes advantage of an ensemble of existing high-resolution climate simulations for a multi-model analysis of the urban climate and its evolution in the Paris region (France). Seven members, based on different Convection-Permitting Regional Climate Models (CP-RCM), provide 10-year simulations for a common historical period and two future periods with the RCP8.5 greenhouse gas emission scenario. The ensemble was analyzed to evaluate the CP-RCMs depending on

the configuration, especially the surface database and land-surface modeling including or not a dedicated urban parameterization (based on a slab approach or an urban canopy model). All urbanized CP-RCMs capture the urban heat island (UHI) and its seasonal variations. A more precise assessment of CP-RCMs according to the type of parameterization remains tricky, and very sensitive to the type and resolution of land cover database. The analysis of projections indicates that all models agree with an increase in heatwave occurrences over Paris region, with greater signal on the natural areas surrounding the city. Most projections suggest a significant mitigation in the daytime UHI at seasonal scale in summer, and a decrease in nighttime UHI during heatwaves. The multi-model approach therefore makes it possible to confirm previous results already obtained by analyses based on a single model.

Keywords

Convection-permitting Regional Climate Models, Multimodel simulations, Urban climate, Heatwaves, Climate change projections.

1 Introduction

Climate change is amplifying weather conditions, leading to an increase in the frequency and intensity of extreme temperature events, and record-breaking heatwaves (IPCC, 2021). Heatwaves are climatic extreme phenomena of great concern due to the high vulnerability of societies to high temperatures. In Europe in particular, the exceptional heatwave of summer 2003 had dramatic health consequences. It resulted in a significant excess mortality in many cities across Europe (Robine et al., 2008), exacerbated locally by the effects of the Urban Heat Island (UHI), as observed in Paris, France (Laaidi et al., 2012). This particularly significant event and the frequent heatwaves observed over the last decade led to a lasting awareness on the society and the public authorities. The urban environment and urban populations are highlighted as particularly vulnerable, making it crucial to properly assess the impacts of climate change in cities and implement appropriate adaptation policies.

Noticeable gaps remain in the literature regarding the analysis of future exposure of urban populations to heatwaves, especially due to the complexity in the processes involved and the interactions of spatial scales. On the one hand, heatwaves are linked to specific large-scale weather patterns characterized by synoptic high-pressure systems driving warm air masses (Perkins, 2015). On the other hand, the local surface conditions, and notably the soil moisture, can influence the intensity or persistence of heatwaves (Sangelantoni et al., 2023; de Vries et al., 2024). In addition, in the case of heatwaves affecting cities, the local influence of urban climate is an additional factor to be taken into account. These interactions between spatial scales and physical processes require a comprehensive and appropriate modeling framework, involving a climate modeling chain for a dynamical downscalling from global to local climate (using limited-area high-resolution regional climate models), as well as dedicated urban parameterizations and databases.

Regional Climate Models (RCMs) are recognized as valuable tools for studying the mechanisms behind heatwaves and their evolution in the context of climate

change over the Mediterranean region (Molina et al., 2020). Despite the major role of GCMs, Molina et al., 2020 pointed out that RCMs simulated the more detailed spatial patterns and features of heatwaves resulting from the regional coastal and orographic effects. Recently, the finer horizontal resolution and improved physics of very high-resolution RCMs, known as Convection-Permitting RCMs (CP-RCMs), have enhanced the representation of small-scale weather mechanisms (Kendon et al., 2021), as well as the surface-atmosphere feedbacks (Knist et al., 2017), compared to coarser-resolution RCMs. According to Sangelantoni et al., 2023, CP-RCMs also improve the representation of warmer/drier conditions than their forcing RCMs (not only during heatwaves), in response to a stronger land-atmosphere coupling in CP-RCMs. When modelling urban areas, improving the horizontal resolution of the models must be accompanied by the implementation of a dedicated surface parameterisation and description. Lemonsu et al., 2023 highlighted the added value of integrating an urban canopy model in the CP-RCM for a realistic simulation of urban processes and associated effects on the spatial contrasts of temperature and precipitation between the city and the countryside. By using a CP-RCM and a bulk parametrisation scheme, Adinolfi et al., 2023 has also shown how this modeling configuration is able to correctly represent the heat released during the summer night hours in terms of minimum temperatures over cities.

Building on these insights, Michau et al., 2024 assessed the exposure of French cities and their rural environments to heatwaves using the CP-RCM AROME (Lucas-Picher et al., 2023) coupled to the urban canopy model TEB (Masson, 2000). Nonetheless, the future increase of heatwaves over urban areas highlighted by Michau et al., 2024 need to be consolidated by the analysis of an ensemble of CP-RCMs. In fact, analyses derived from CP-RCM ensembles, carried out for example in the field of convection (*e.g.* Fosser et al., 2024) and wind speed (*e.g.* Molina et al., 2024), have proven their advantages and robustness. The present study is based on an ensemble of CP-RCMs simulations carried out in the CORDEX FPS-Convection project (CORDEX Flagship Pilot Study on Convective Phenomena over Europe and the Mediterranean, Coppola et al.,

2020). The Paris region is here used as a case study for the intercomparison of CP-RCMs. Several factors make the city of Paris ideal for developing an multi CP-RCM intercomparison. Paris is one of Europe's major cities, with an extensive urban area and a fairly simple geographical location (relatively flat topography and no coastline), which means that the results can be interpreted with a focus on urban aspects.

In this study, the ensemble of CP-RCM simulations is analyzed to investigate and quantify the evolution of the urban climate in response to global warming, and to project long-term changes in the exposure of Paris urban population to heatwaves. It should be noted that this work contributes to the CORDEX FPS URB RCC (CORDEX Flagship Pilot Study on URBan environments and Regional Climate Change, Langendijk et al., 2024) community to improve our understanding of the interactions between regional and urban climates. In this context, a major challenge of this study is to exploit the current CP-RCM ensemble of climate simulations to draw scientific findings, but also to clarify the experimental setup requirements (modeling chain, surface databases, or the need of a surface energy balance model specific to the urban environment) for future intercomparisons.

The next section presents the models and simulations used in the multi-model analysis, as well as the climate indicators selected to assess the vulnerability of urban and rural areas to global warming. In section 3, we analyze the evolution of the indicators, including temperature, UHI intensity, the heatwave characteristics for all the climate simulations. Finally, section 4 provides a summary and conclusion based on our findings.

2 Materials and methods

2.1 Models and simulations

For the present study, seven CP-RCM climate simulations have been selected from the set of simulations carried out as part of the CORDEX FPS-Convection

project (Coppola et al., 2020). They were run on a common domain centered over the Alps (ALP-3), with grid spacing between 2.5 and 4 km, and covered a common historical period and at least one future medium- or long-term horizon (Table 1). These seven simulations have been produced with a spatial dynamical downscaling starting from CMIP5 GCM simulations based on RCP8.5 greenhouse gas (GHG) emission scenario, and all including an intermediate RCM. They used four different CP-RCMs: two simulations have been produced with WRF (Skamarock and Klemp, 2008), two with COSMO-CLM (Rockel et al., 2008), two with AROME (Belušić et al., 2020; Caillaud et al., 2021), and one with RegCM4 (Coppola et al., 2021; Pichelli et al., 2021).

A complete description of the dynamics and physics of these CP-RCMs is presented by Ban et al., 2021 as part of a wider group of CP-RCMs that have been evaluated. Here, a description of the CP-RCM configurations is provided, focusing on the representation of urban areas *i.e.*, the choice of surface schemes and urban parameterizations, as well as the land cover databases.

Table 1. Climate modeling configurations used in the study.

Name	Institute	GCM	RCM	CP-RCM	Simulation period
WRF-BCCR-AUTH	BCCR	NorESM1-ME (Bentsen et al., 2013)	WRF381DA (EUR-15, 15 km) (Skamarock and Klemp, 2008)	WRF381DA (ALP-3, 3 km) (Skamarock and Klemp, 2008)	1996-2005 / /
WRF-BCCR-AUTH	AUTH	NorESM1-ME (Bentsen et al., 2013)	WRF381DA (EUR-15, 15 km) (Skamarock and Klemp, 2008)	WRF381DA (ALP-3, 3 km) (Skamarock and Klemp, 2008)	/ / 2090-2099
WRF-IPSL	IPSL	IPSL-CM5A-MR r1 (Dufresne et al., 2013)	WRF381CE (EUR-15, 15 km) (Skamarock et al., 2008)	WRF381CE (ALP-3, 3 km) (Skamarock et al., 2008)	1996-2005 2041-2050
CCLM-BTU	BTU	CNRM-CM5 r1 (Voldoire et al., 2012)	CCLM4-8-17 (EUR-11, 12 km) (Keuler et al., 2016)	CCLM5-0-14 (ALP-3, 3 km) (Rockel et al., 2008)	1996-2005 2041-2050 2090-2099
CCLM-CMCC	CMCC	EC-EARTH r12 (Hazeleger et al., 2011)	CCLM5-0-9 (EUR-11, 12 km) (Rockel et al., 2008)	CCLM5-0-9 (ALP-3, 3 km) (**Adinolfi2021**)	1996-2005 2041-2050 2090-2099
AROME-CNRM	CNRM	CNRM-CM5 r1 (Voldoire et al., 2012)	CNRM-ALADIN63 (MED-11, 12 km) (Nabat et al., 2020)	CNRM-AROME41t1 (ALP-3, 2.5 km) (Caillaud et al., 2021)	1996-2005 2041-2050 2090-2099
AROME-KNMI	KNMI	EC-EARTH r14 r04 r13 (Hazeleger et al., 2011)	RACMO23E (WCE-11, 12 km) (van Meijgaard et al., 2012)	HCLIM38h1-AROME (ALP-3, 2.5 km) (Belušić et al., 2020)	1996-2005 2041-2050 2090-2099
RegCM-ICTP	ICTP	HadGEM2-ES r1 (Jones et al., 2011)	RegCM4-7-1 (EUR-11, 12 km) (Giorgi et al., 2012)	RegCM4-7-1 (ALP-3, 3 km) (Coppola et al., 2021)	1995-2005 2040-2049 2090-2099

Table 2. Surface modeling configurations used in the study.

Name	Institute	Land cover database	Land surface scheme	Urban parametrization
WRF-BCCR-AUTH	BCCR/AUTH	CORINE Land Cover 2006	NOAH-MP [single class] (Niu et al., 2011)	Slab
WRF-IPSL	IPSL	CORINE Land Cover 2006	NOAH [single class] (Ek et al., 2003)	UCM (Kusaka et al., 2001)
CCLM-BTU	BTU	GLC2000 (Bartholomé and Belward, 2005)	TERRA-ML [tiles] (Schrodin and Heise, 2001)	No urban
CCLM-CMCC	CMCC	GLC2000 (Bartholomé and Belward, 2005)	TERRA-ML [tiles] (Schrodin and Heise, 2001)	TERRA-URB v1 (Wouters et al., 2015)
AROME-CNRM	CNRM	ECOCLIMAP-I (Champeaux et al., 2005)	SURFEX [tiles] (Masson et al., 2013)	TEB (Masson, 2000)
AROME-KNMI	KNMI	ECOCLIMAP-II (Faroux et al., 2013)	SURFEX [tiles] (Masson et al., 2013)	TEB (Masson, 2000)
RegCM-ICTP	ICTP	MODIS and LandScan 2004 (Yang et al., 2006) (Dobson et al., 2000)	CLM4.5 [tiles] (Oleson and Lawrence, 2013)	CLMU (Oleson et al., 2010)

For the seven selected CP-RCMs simulations, two types of urban parametrizations with varying levels of complexity have been used. For the slab-type models, the urban areas are considered as flat surfaces for which surface properties are modulated to approximate real urban characteristics (*e.g.* high surface roughness, low albedo, anthropogenic heat emissions). Depending on the approach, this may involve a dedicated urban parameterisation or an adaptation of the existing Soil-Vegetation-Atmosphere Transfer scheme. The Urban Canopy Models (UCM) provide a more realistic description of urban geometry and separate the various elements of the urban canyon (road, roof, walls). The radiative, energetic and turbulent exchanges between the urban areas and the atmosphere are calculated, taking into account the effects of shading, radiative trapping and drag of buildings. Unlike the slab approach, an air temperature is calculated within the urban canyon.

WRF

The version 3.8.1 of WRF (Skamarock et al., 2008) with a horizontal resolution of 3 km has been used for two different experiments. The Bjerknes Centre for Climate Research (BCCR) and the Aristotle University of Thessaloniki (AUTH) has collaborated to conduct joint experiments (hereinafter referred to as WRF-BCCR-AUTH), covering both the historical 1996-2005 and the end-of-century period 2090-2099 periods. An intermediate 15-km WRF simulation was forced at its lateral boundaries with the GCM NorESM1-ME (Bentsen et al., 2013). Another WRF climate simulation (hereinafter referred to as WRF-IPSL) was conducted by the Institute Pierre Simon-Laplace (IPSL). An intermediate 15-km WRF simulation was forced by the GCM IPSL-CM5-MR (Dufresne et al., 2013). The WRF-IPSL experiments cover the historical period 1996-2005 and the medium-term period 2041-2050.

Land surface processes are simulated using the NOAH surface scheme (Ek et al., 2003) in WRF-IPSL or using the more sophisticated NOAH-MP surface scheme (NOAH Multi-Parameterization, Niu et al., 2011) in WRF-BCCR-AUTH configuration. The latter allows a more detailed representation of ground-related

processes compared to the previous version (Ban et al., 2021). The representation of urban areas also differs in the two experiments: WRF-BCCR-AUTH uses a simple slab-type parameterization associated with specific surface parameters to reflect urban cover characteristics (albedo, emissivity, thermal properties, surface roughness), whereas WRF-IPSL relies on the single-layer urban canopy model (UCM) described by Kusaka et al. (2001). In WRF experiments, the land-use and land-cover database is based on the 2006 CORINE Land Cover.

COSMO-CLM

The Brandenburg University of Technology (BTU) and the Centro Euro-Mediterraneo sui Cambiamenti Climatici (CMCC) have both used the RCM COSMO-CLM (Rockel et al., 2008) at 3-km horizontal resolution, but from the two different versions 5.0.9 and 5.0.14, respectively. These experiments are subsequently referred to as CCLM-BTU and CCLM-CMCC. BTU used version 4.0.17 of CCLM and the GCM CNRM-CM5 (Voldoire et al., 2012) to force an intermediate 12-km CCLM-RCM. CMCC used version 5.0.9 of CCLM and the GCM EC-EARTH (Hazeleger et al., 2011) to force an intermediate 12-km RCM. Both experiments cover the three time periods of interest *i.e.*, 1996-2005, 2041-2050, and 2090-2099.

Both experiments use the same TERRA-ML land-surface model (TERRA Multi-Layer, Schrodin and Heise, 2001), which resolves the soil column into eight vertically stretched layers (Doms et al., 2005). CCLM-BTU is the only experiment of the ensemble that does not incorporate any specific parameterization to represent urban areas that are modeled as natural covers. In contrast, CCLM-CMCC uses the TERRA-URB parameterization. This slab-type parameterization is enhanced, notably considering additional parameters such as anthropogenic heat flux (Wouters et al., 2015). Surface characteristics are provided by the GLC2000 land-use and land-cover database (Bartholomé and Belward, 2005).

AROME

Different CP-RCM AROME versions are developped by the Centre National de Recherches Météorologiques (CNRM) and the Royal Netherlands Meteorological Institute (KNMI) at a 2.5-km horizontal resolution. The notable differences between these versions and configurations of AROME are detailed by Belušić et al., 2020. The experiment AROME-CNRM follows the cycle 41t1 of AROME, as described in Caillaud et al., 2021. AROME-CNRM is driven by an intermediate RCM CNRM-ALADIN v6 (Nabat et al., 2020) simulation that is forced by the GCM CNRM-CM5 (Voldoire et al., 2012). The experiment AROME-KNMI follows the cycle 38 of AROME described in Belušić et al. (2020). AROME-KNMI is driven by an intermediate RCM RACMO23E (van Meijgaard et al., 2008; van Meijgaard et al., 2012) simulation that is forced by the GCM EC-EARTH (Hazeleger et al., 2011). The AROME-CNRM and AROME-KNMI experiments cover three 10-year time periods 1996-2005, 2041-2050, and 2090-2099.

The land surface scheme used by the AROME experiments is SURFEX (Masson et al., 2013), following version 7.2 for AROME-CNRM and for AROME-KNMI with differences in snow and soil parameterizations in particular (D95 snow scheme by Douville et al., 1995 and ISBA 3-L by Boone et al., 1999 for AROME-CNRM, and multi-layer snow scheme ISBA-ES by Decharme et al., 2016 and ISBA-DIFF by Decharme et al., 2011 for AROME-KNMI). For the representation of urban areas and the calculation of radiation, energy, and momentum fluxes, both AROME configuration activated the original version of the urban canopy model Town Energy Balance (TEB) without vegetation in the canyon (Masson, 2000). For AROME-KNMI, the air layer in the canyon is parameterized and the air temperature is calculated at mid-height of the buildings according to method of Masson, 2000. For AROME-CNRM, the CANOPY option (Hamdi and Masson, 2008) allows a vertical discretisation of the air layer in the canyon using a simplified boundary layer model. Finally, the land-use and land-cover databases are ECOCLIMAP-I (Champeaux et al., 2005) for AROME-CNRM and ECOCLIMAP-II (Faroux et al., 2013) for AROME-KNMI, for which the urban cover differs particularly.

Reg-CM4

The Abdus Salam International Centre for Theoretical Physics (ICTP) develops the RegCM RCM (Giorgi et al., 2012). In this study, we used a simulation produced by the RegCM version 4.7.1 at 3-km resolution that is detailed in Coppola et al. (2021). For this experiment, referred to as RegCM-ICTP, the GCM HadGEM2-ES (Jones et al., 2011) provides the lateral boundary conditions to the intermediate 12-km RCM RegCM4-7-1 (Giorgi et al., 2012), which then forced the 3-km CP-RCM RegCM. The experiments cover the historical 1995-2005 period, and the mid- and long-term horizons 2040-2049 and 2090-2099 periods, respectively.

The atmospheric model of RegCM is coupled with the surface scheme CLM4.5 (Oleson and Lawrence, 2013) in which the equations for water and energy balances are solved for each land cover type using specific schemes, and then aggregated at the grid level. The main land cover types include glaciers, lakes, vegetation, and crops, with characteristics obtained from MODIS (Yang et al., 2006), as well as urban areas based on the LandScan 2004 dataset (Dobson et al., 2000). In particular, the urban areas in the surface scheme CLM4.5 are represented using the single-layer urban canopy model CLMU (Community Land Model Urban, Oleson et al., 2010).

2.2 Urban and natural masks

The surface modeling is very different from one CP-RCM to another. The CP-RCMs use surface schemes of different levels of complexity and different urban parameterizations. Moreover, different datasets are used by the CP-RCMs to take into account the land-use and its conversion into surface properties. In order to compare fairly the models with regard to surface processes in an urban environment, the native grid of each CP-RCM is retained to preserve the surface information integrity (without interpolating the simulations on a common grid).

Establishing a common methodology for deriving urban and rural temperatures from each model using consistent spatial masks specific to each CP-RCM

is particularly challenging. The methodology applied here consists in defining urban and natural masks over the region of Paris following the approach of García-Nieto et al. (2018). The Paris urban area is bounded by a circle with a radius of 20 km (R_{urb}) corresponding to the surface area A_{urb}. The rural area is defined by the peripheral zone of the urban area defined as a ring of minimum radius $R_{rur1} = R_{urb} + 0.25\sqrt{A_{urb}}$ and maximum radius $R_{rur2} = R_{urb} + 1.5\sqrt{A_{urb}}$. Then, the properties of the land surface from each CP-RCM are used to exclude from the urban and natural areas the cells for which the type of cover does not match with those from the masks considered (Figure 1).

The CCLM-BTU, CCLM-CMCC, WRF-BCCR-AUTH and WRF-IPSL models apply a predominant surface cover approach. Based on the type of surface cover from the selected databases (GCL2000 for both CCLM experiments and CORINE Land Cover 2006 for both WRF experiments) that is interpolated on the CP-RCM 3-km grid, the predominant land-cover class is selected for each grid cell. It is then straightforward to exclude urban cells from the natural mask, and natural cells from the urban mask (see Figure 1). The other models applied a tiling approach that is commonly used for land-surface modeling. According to this approach, each cell is divided in fractions of different covers (*e.g.* water, sea, urban, nature) coming from the land-cover database. Therefore, thresholds need to be defined for the coverage fractions in the grid cells in order to distinguish urban pixels from natural pixels. A sensitivity analysis allowed us to set the minimum threshold at 60 % for the urban fraction resulting in urban areas of fairly comparable size for all CP-RCMs. For the natural masks, cells for which the urbanization threshold is reached are excluded (see Figure 1).

The number of pixels in each urban and natural mask is shown in Figure 1. The size of the natural masks is fairly comparable between the models, varying from around 12900 km^2 to 14000 km^2. For the urban masks, there are more significant differences, with sizes ranging from 440 km^2 to over 1200 km^2. In particular, we note a very compact urban mask for RegCM-ICTP due to the land use database used.

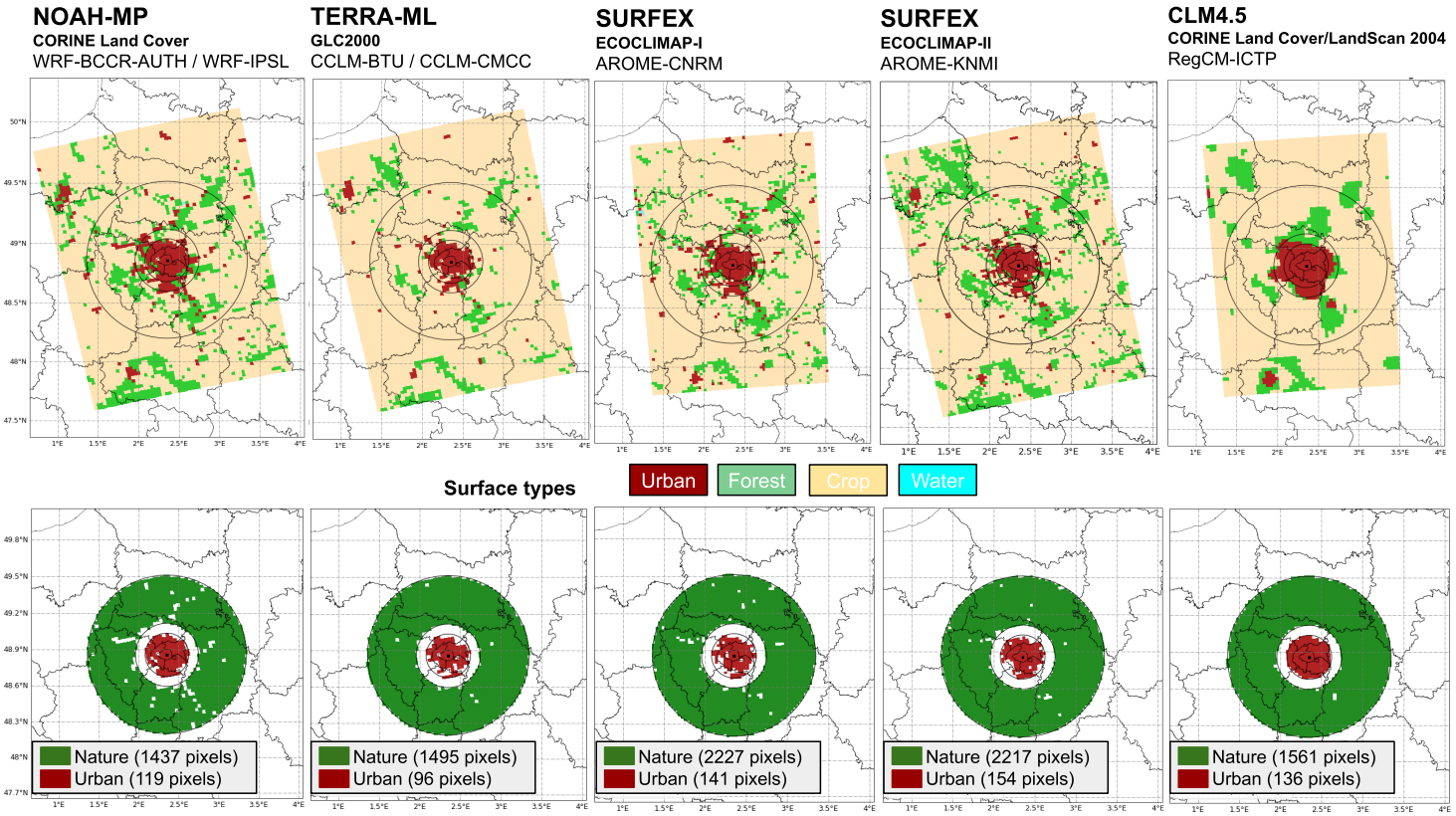

Figure 1. (Top) Spatial distribution of the 4 main surface types (artificial in red, forest in green, agricultural in yellow, and water in blue) for different models. (Bottom) Definition of urban (in red) and nature (in green) masks calculated from the different models. From left to right, the configurations of the different models are namely the (`NOAH-MP/NOAH`, `TERRA-ML`, `SURFEX`, and `CLM4.5`) and their associated land cover databases (`CORINE Land Cover 2006`, `GLC2000`, `ECOCLIMAP-I`, `ECOCLIMAP-II`, `CORINE Land Cover/LandScan 2004`).

2.3 Climate indicators and analysis method

The meteorological variables from the CP-RCMs used in this study are the daily minimum (TN) and maximum (TX) temperatures. The daily mean temperature (TM) is computed averaging together TN and TX (TM not being directly available). Urban and rural temperatures are determined on the basis of the urban and natural masks defined earlier for each model (Section 2.2). The intensity of the nocturnal urban heat island (UHIN) is calculated as the difference between the minimum temperature averaged over the urban mask and that averaged over the natural mask, as follows: $UHIN = \overline{TN_{URB}} - \overline{TN_{RUR}}$. The same is done for the intensity of the daytime urban heat island (UHIX) using the maximum temperature.

TN and TX of the natural mask are used to characterize regional climate conditions over the Paris region during the historical period (HIST, corresponding to the period 1996-2005). Not taking urban grid points into account means that climate trends are analyzed without potential urban influences, - at this stage of the analysis -. Simulated temperatures during HIST of the ensemble and individual CP-RCMs are compared with the observed ANASTASIA dataset (a gridded dataset of daily minimum and maximum temperatures at a 1 km horizontal resolution over metropolitan France covering the period 1947-2016, Besson et al., 2019) for evaluation purposes. It should be noted that this database is unable to accurately represent the influence of urban areas on climate, as the kriging method used to develop the product does not take into account a large number of urban weather stations.

Future trends of regional climate conditions of the ensemble and individual CP-RCMs are analyzed for both the medium-term (MT, 2041-2050) and the long-term (LT, 2090-2099) periods, relative to the HIST period (1996-2005). Climate projections were produced using the RCP8.5 greenhouse gases concentration scenario

An additional analysis focuses on the evolution of heatwaves and their characteristics (maximum intensity, duration, and severity) between HIST period and

the two future periods, following the approach already implemented by Michau et al. (2024). As a reminder, the heatwaves are detected in accordance with the definition of Ouzeau et al. (2016). Three different thresholds as quantiles 99.5, 97.5, and 95 (for peak, beginning and end of heatwave respectively) are applied on long timeseries of daily mean temperature (TM) by considering the entire time series (not just JJA days). This approach is applied to the simulated timeseries of TM, indepedantly for each CP-RCM, and by distinguishing urban and natural environments (*i.e.* on temperature over the urban or rural mask).

3 Results and discussions

3.1 Minimal and maximal temperatures

3.1.1 Evaluation of the CP-RCMs over the historical period

Figure 2 presents the daily distributions of TN_{RUR} and TX_{RUR} simulated by each CP-RCM over HIST period, as well as the multi-model ensemble mean, in the different season. These values are compared to the observed distribution provided by the ANASTASIA observation dataset for the same period. The analysis is restricted to the natural mask to investigate regional trends, avoiding urban influences. The distribution of ANASTASIA illustrates the climatology of the region of Paris that corresponds to a semi-oceanic climate, with significant variations in TN and TX across the seasons.

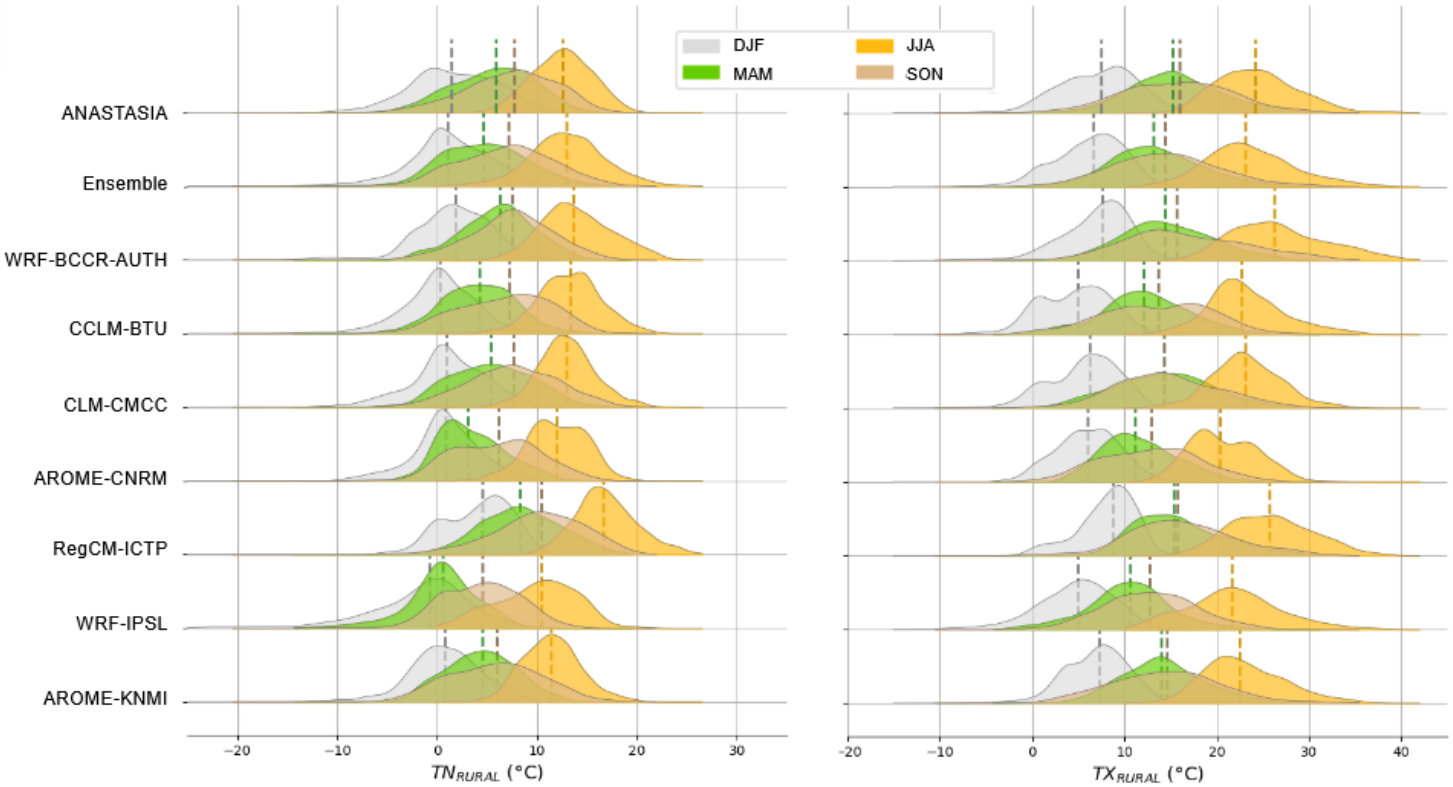

Figure 2. Daily distributions of TN (left) and TX (right) in the natural environment during HIST period, observed in the ANASTASIA product and simulated by the ensemble and each individual CP-RCM, in the different season. Winter (DJF), spring (MAM), summer (JJA), and autumn (SON) seasons are represented by the colors gray, green, yellow, and brown, respectively. Dashed lines illustrate the medians of each distribution.

CP-RCM experiments exhibit diverse performances, as illustrated in Figure 2. RegCM-ICTP considerably overestimates TN in all seasons, with median biases equal to or exceeding +2.4 °C (with a maximum bias in DJF). Conversely, WRF-IPSL underestimates TN, with biases of the median from -2.2 °C in DJF and JJA to -5.3 °C in MAM, with pronounced cold extremes in DJF and JJA. Although less significant, cold biases are also seen in the seasonal distributions of TN for AROME-KNMI, CCLM-BTU, and AROME-CNRM with values ranging from -0.6 °C to -2.8 °C. CCLM-CMCC and to a lesser extent WRF-BCCR-AUTH are the models that most faithfully reproduce TN, with median biases ranging ±0.5 °C, except in JJA for WRF-BCCR-AUTH. The seasonal distributions for the ensemble mean of TN are quite realistic, indicating of error compensation from each model. The main defects are the too cold TN in MAM (primarily attributable to WRF-IPSL and AROME-CNRM).

For TX, positive biases of the medians are evident in JJA for WRF-BCCR-AUTH (+2.1 °C) and RegCM-ICTP (+1.6 °C), along with pronounced warm extremes. RegCM-ICTP is also too warm in DJF, with a median bias of +1.2 °C. On the other hand, the other models tend to underestimate TX, with median biases ranging from -0.8 °C to -4.7 °C, with a significant cold bias for AROME-CNRM in JJA. Consequently, the ensemble mean exhibits a cold bias for all seasons, with median biases ranging between -1.0 °C and -2.3 °C, with the most pronounced bias during MAM.

In this analysis, RegCM-ICTP stands out with the higher temperatures compared to the other models and observations. These discrepancies could be attributed to systematic biases inherent in the forcing RCM or GCM. According to Vautard et al. (2021), the forcing GCM contributes more than the RCM itself for TX, but for TN, the most important contribution is the RCM. For TX, the warm biases for RegCM-ICTP could be associated with the HadGEM2-ES GCM (Collins et al., 2008). However, drawing definitive conclusions about the causes of the biases is challenging without further analysis, as the CP-RCMs used different RCM and GCM forcings.

3.1.2 Projected minimum and maximum temperatures

Summer maps of TN and TX simulated by all CP-RCMs over HIST period are shown in Figure 3 and Figure 4, together with the difference maps of TN and TX between the MT and LT horizons (using RCP8.5 GHG emission scenario) and HIST period. As a reminder, six models are available for the MT horizon (all except WRF-BCCR-AUTH), and six models for the LT horizon (all except WRF-IPSL).

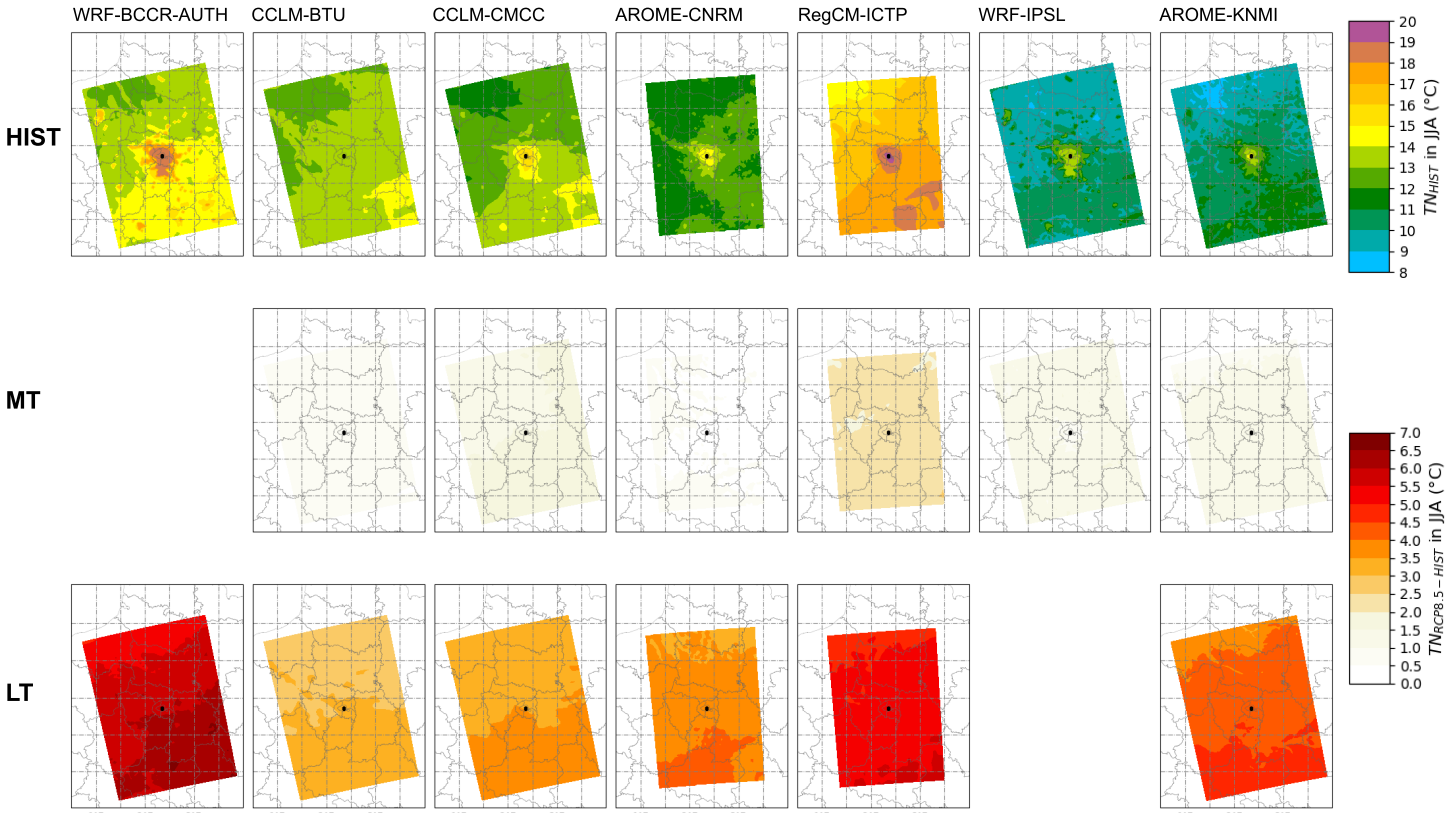

Figure 3. Summer TN during HIST period (top) simulated by each individual CP-RCM. Differences between MT and HIST period (middle), as well as between LT and HIST period (bottom) simulated by each individual CP-RCM.

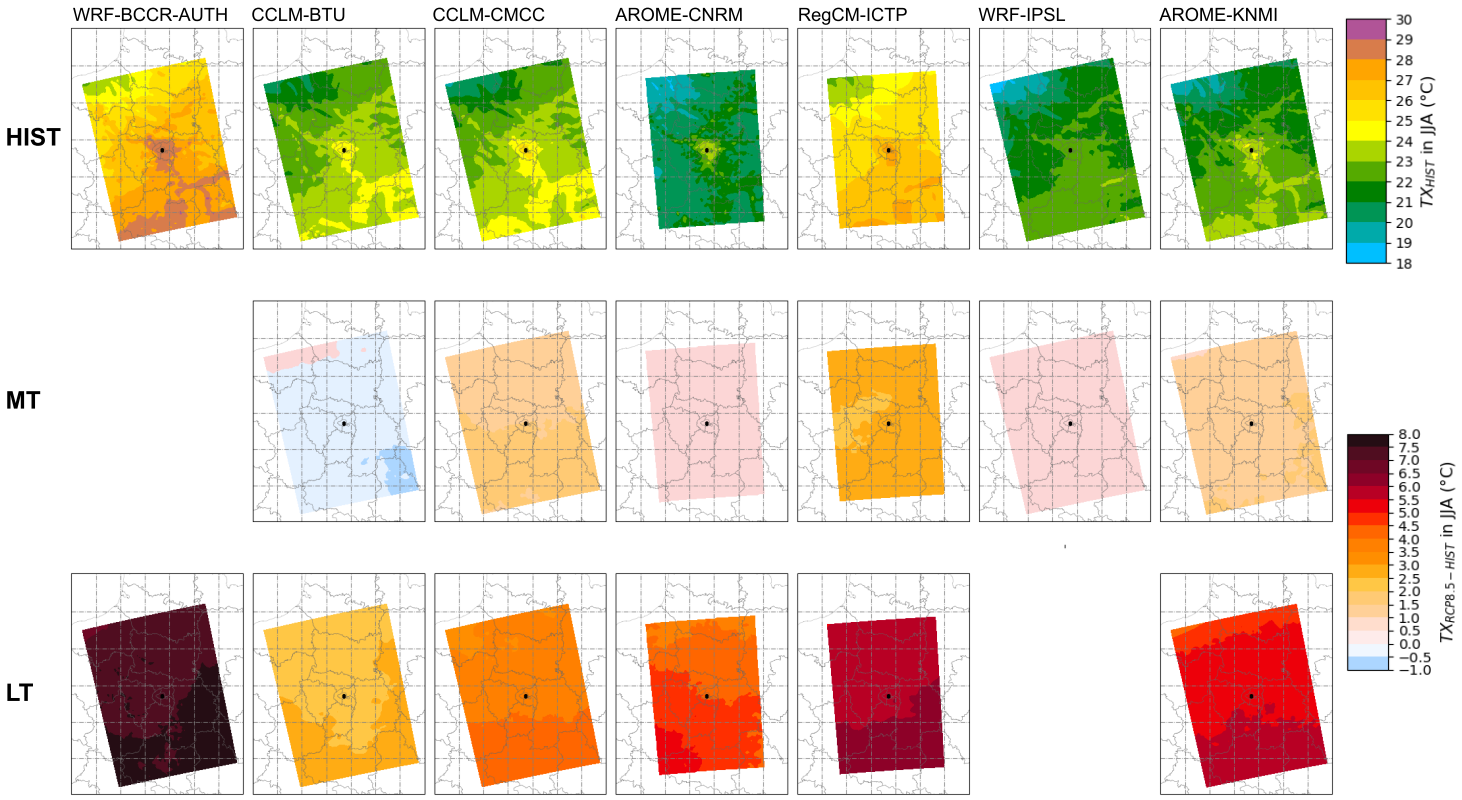

Figure 4. Summer TX during HIST period (top) simulated by each individual CP-RCM. Differences between MT and HIST period (middle), as well as between LT and HIST period (bottom) simulated by each individual CP-RCM.

The TN and TX maps for summer (JJA) in HIST period show the temperature differences between the CP-RCMs, in line with the distributions already discussed. They also show the regional contrasts in the study area, between the south-east and the north-west. Finally, they highlight the city's signal on TN and TX, which varies in strength depending on the model (this will be discussed later). Note that CP-RCMs are not compared with observations here, as there are no data covering the entire area and enabling accurate representation of temperatures in urban areas over HIST period. As a reminder, the ANASTASIA product used earlier in the study is unable to accurately represent the influence of urban areas on climate, as the method used to develop the product does not take into account a large number of urban weather stations.

Over the 10-year MT period, the ensemble mean projects a warming of +1.2 °C in TN (with a range of +0.5/+2.2 °C) and of +0.9 °C in TX (with a range of -0.3/+2.6 °C depending on the model). The warming increases significantly by the end of the century (LT period), reaching +4.3 °C in TN (with a range of +3.0/+5.9 °C) and of +4.9 °C in TX (with a wider range of +2.4/+7.5 °C depending on the models). CCLM-BTU projects the smallest warming for both TN and TX. Conversely, WRF-BCCR-AUTH projects the strongest warming for both TN and TX.

According to Figures 3 and 4, the CP-RCMs suggest a warming at the regional scale, without any spatial pattern of accentuated warming at the urban level (as in de Vries et al. (2024)). For the two future periods, but more clearly for LT, the analyses reveal that the north to south spatial gradient of TN in JJA is reinforced compared to HIST period for all models.

3.2 Nocturnal and diurnal urban heat islands

3.2.1 Evaluation of the CP-RCMs over the historical period

The seasonal UHIN and UHIX indicators for HIST period, calculated respectively as the difference in TN and in TX between urban and natural areas, are presented and compared for all CP-RCMs in Figure 5 (left panel).

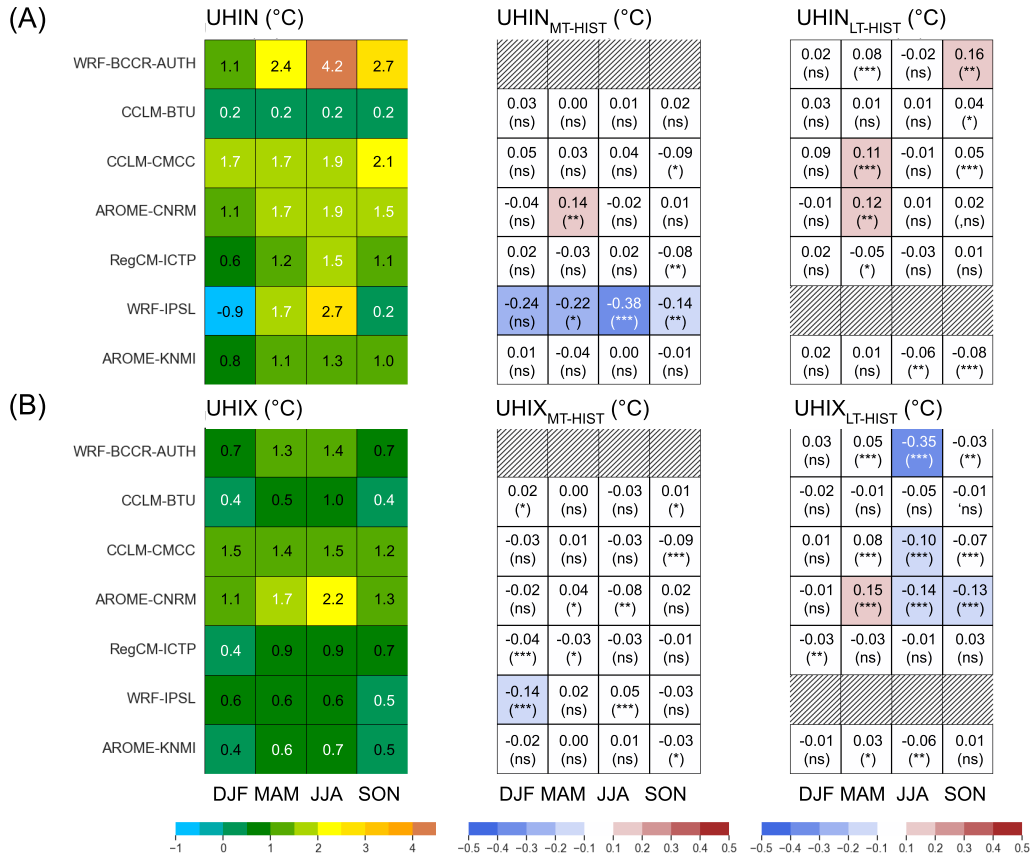

Figure 5. (A) Nocturnal (top) and diurnal (bottom) median daily UHIs (in °C) for each CP-RCM in the different season.(B) Variation in median daily UHIs (in °C) for each CP-RCM between MT and HIST periods (on the left), as well as between LT and HIST periods (on the right) in the different season. Differences between distributions were assessed using the Mann-Whitney non-parametric test adapted for independent samples with hypotheses H0 (medians are equal) and H1 (medians are different). Symbols refer to the following significance thresholds: ***: 1e-4 $\leq$ p-value $\leq$ 1e-3, **: 1e-3 $\leq$ p-value $\leq$ 1e-2, *: 1e-2 $\leq$ p-value $\leq$ 0.05, ns (not significant): 0.05 $\leq$ p-value $\leq$ 1.

Firstly, we note the differentiated behaviour of CCLM-BTU, which has systematically lower UHIN and UHIX values than all the other CP-RCMs, which is consistent with the fact that it is the only model not to represent urban areas. Nevertheless, UHIN are slightly positive for all seasons (0.2 °C) and UHIX slightly higher (between 0.4 and 1.0 °C), that could result from differences in surface properties between urban and natural cells. However, we do not have specific information on these surface properties. The other CP-RCMs, that incorporate a representation of urban areas (using simple slab model or more sophisticated UCM), all simulate positive UHIX and UHIN for HIST period (except WRF-IPSL in DJF) with intensities varying from one model to another. In the vast majority of cases, they simulate stronger UHIN than UHIX, which is consistent with the literature and our knowledge of the physical processes involved in the development of urban heat island, which is a typically nocturnal phenomenon (Oke et al., 2017). Only AROME-CNRM simulates an UHIX that is slightly stronger than the UHIN, in JJA.

The results also show a pronounced seasonal variation, especially during the night, with a minimum in DJF and a maximum in JJA. Again, this corresponds to what is expected, since the UHI intensity is strongly governed by the incoming solar radiation, which favours the heat storage in urban infrastructures (Oke et al., 2017). Only CCLM-CMCC simulates a maximum UHIN in SON (2.1 °C) but with value close to that in JJA (1.9 °C). The dispersion of UHIN and UHIX intensities between the models is relatively high, even when the analysis is limited to CP-RCMs that incorporate a specific urban surface parameterization. For instance, RegCM-ICTP shows an UHIN of 1.5 °C in JJA against 4.2 °C for WRF-BCCR-AUTH. It is noteworthy that WRF-IPSL stands out significantly by displaying a near zero and even negative UHIN in SON and DJF, respectively.

3.2.2 Change of urban heat islands with climate change

The seasonal differences in UHIN and UHIX calculated between the two future periods MT and LT and the HIST period are presented in Figure 5 (middle and right panels). For MT period, most models do not show significant differences

at the 95 % confidence level, whether for UHIN or UHIX (differences between -0.1 and 0.1 °C). However, WRF-IPSL projects a significant decrease in MAM (-0.22 °C), JJA (-0.38 °C), and SON (-0.14 °C) for UHIN, as well as in DJF (-0.14 °C) for UHIX. To the contrary, UHIN simulated by AROME-CNRM presents a significant increase in MAM (+0.14 °C) in TN.

The change of the UHI becomes more pronounced in LT than in MT, and significant for a larger number of models (Figure 5, right panel). However, there is little agreement on the changes between the models. This is particularly the case for seasonal UHINs. In DJF, no significant change is found for all models. In MAM, CCLM-CMCC and AROME-CNRM agree on a significant increase of +0.11 °C and +0.12 °C, respectively. In JJA, only AROME-KNMI indicates a significant decrease in UHIN of -0.06 °C. Finally, in SON, AROME-KNMI projects a decrease of the UHIN (-0.08 °C) that is close to that in JJA, but WRF-BCCR-AUTH shows a significant increase of +0.16 °C of UHIN. Regarding UHIX, WRF-BCCR-AUTH, CCLM-CMCC, AROME-CNRM, and AROME-KNMI agree on a significant decrease (with variations down to -0.35 °C for WRF-BCCR-AUTH) in JJA. No significant change is noted for the other seasons for most of the models. Only CNRM-AROME shows an increase of the UHIX in MAM (+0.15 °C) followed by a decrease in JJA and SON (-0.14 °C and -0.13 °C, respectively).

3.3 Heatwaves

In this section, the future changes of heatwave characteristics are analyzed, distinguishing urban and natural environments (as done by Michau et al., 2024). Using quantile thresholds for heatwave detection provides a new perspective on the ability of the different CP-RCMs to simulate hot extremes of temperature. The three quantile thresholds (99.5, 97.5, and 95) used to detect heatwaves according to the Ouzeau et al. (2016) method are determined for ANASTASIA observations and for each CP-RCM both for HIST period and on the natural mask. The values are compiled in Table 3.

Table 3. Comparison of TM quantiles 99.5 (S1), 97.5 (S2) and 95 (S3) in °C calculated for each model, for the observed ANASTASIA dataset over the HIST period for the natural mask, and for the urban weather station over the HIST period. In addition, the difference between the quantiles calculated for the urban mask and for the natural mask is indicated in brackets.

	S1 (°C)	S2 (°C)	S3 (°C)
Observations	26.7 (+0.7)	22.6 (+2.0)	21.4 (+1.8)
WRF-BCCR-AUTH	29.3 (+3.3)	26.8 (+3.0)	24.3 (+2.9)
CCLM-BTU	26.2 (+0.7)	22.9 (+0.8)	20.9 (+0.6)
CCLM-CMCC	25.3 (+1.9)	22.3 (+1.7)	20.8 (+1.9)
AROME-CNRM	22.6 (+2.6)	20.6 (+2.4)	19.5 (+2.3)
RegCM-ICTP	29.4 (+1.8)	26.2 (+1.5)	24.4 (+1.5)
WRF-IPSL	24.1 (+2.3)	21.0 (+1.9)	19.3 (+1.6)
AROME-KNMI	25.6 (+1.1)	22.0 (+1.2)	20.2 (+1.1)

Compared with ANASTASIA, WRF-BCCR-AUTH and RegCM-ICTP show higher temperature for all quantiles in the natural environment. As in previous analyses, these models stand out as particularly hot. On the contrary, AROME-CNRM and to a lesser extent AROME-KNMI and WRF-IPSL show lower temperature quantiles compared to those observed. CCLM-BTU and to a lesser extent CCLM-CMCC realistically simulate extreme heat conditions, with values close to those of ANASTASIA (difference of ± 1 °C for the different quantiles). As expected, the same quantile thresholds, this time calculated for the urban mask (Table 3, values in brackets), are much higher than for the natural mask due to urban influences. This is the case for all the models except for CCLM-BTU, which has no representation of urban areas.

The average number of heatwave days per year, as well as the duration of heatwaves, calculated for each CP-RCM over the HIST and future (MT and LT) periods, and for both the urban and natural environements, are presented in Figure 6.

(a) Average number of heatwave days per year.

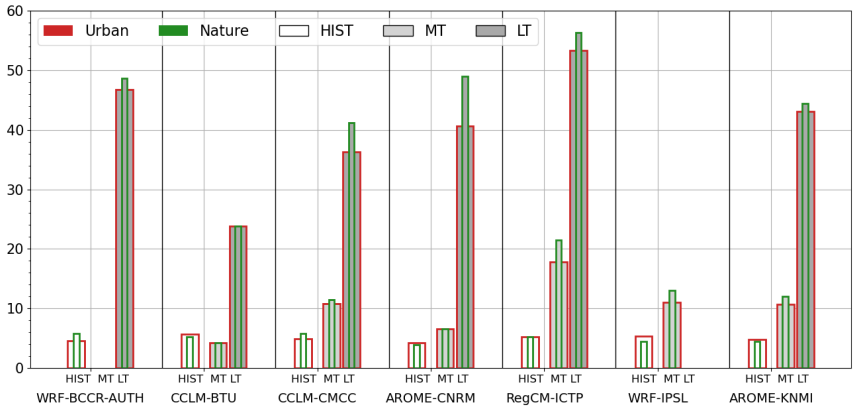

(b) Duration (in days) of heatwaves.

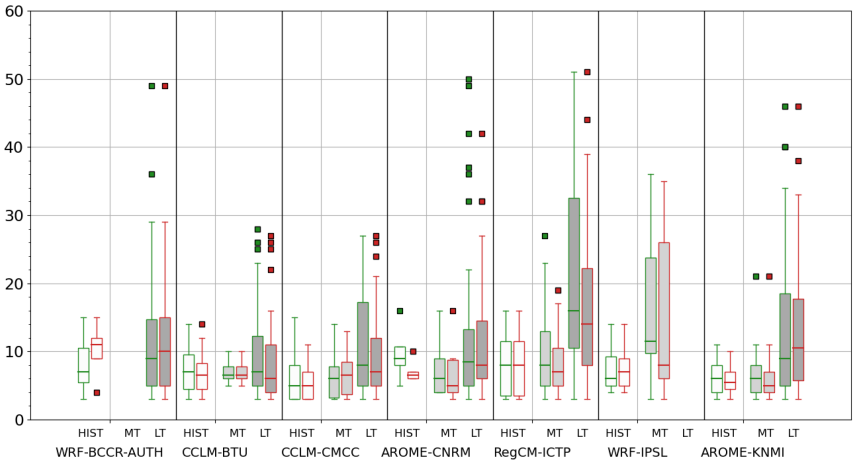

Figure 6. Indicators characterizing heatwaves in urban (in red) and natural (in green) environments in HIST (white), MT (light grey), and LT (dark grey) periods. The box extends from the first quartile (Q1) to the third quartile (Q3) of the data, with a line at the median. The whiskers extend from the box to the farthest data point lying within 1.5x the inter-quartile range (IQR) from the box. Flier points are those past the end of the whiskers.

For the HIST period, as induced by the heatwave definition, the models simulate a fairly comparable number of heatwave days on average over the year, of the order of 5 days per year (Figure 6a). The differences of heatwave days between urban and natural areas are less than ± 0.5 days per year, except for the WRF-BCCR-AUTH, CCLM-CMCC, and WRF-IPSL experiments (differences of -1.2, -0.9, and +0.8 days per year, respectively). The above results were expected since they are directly linked to the heatwave detection quantiles that are different for urban and natural environments. The median durations of heatwaves vary between 5 and 9 days between models, with some events lasting more than 10 days and up to 2 weeks (Figure 6b). Most of models show very small differences between urban and natural environments. Nonetheless, WRF-BCCR-AUTH simulates shorter heatwaves for natural areas than for urban areas, and inversely AROME-CNRM simulates longer heatwaves for urban areas than for natural areas.

With climate change, the average number of heatwave days per year changes by a factor of 0.7 to 3.4 for the MT and by a factor of 4.2 to 11.1 for the LT periods (Figure 6a). At the end of the century, significant differences in number of heatwave days are noted between models. WRF-AUTH-BCCR and RegCM-ICTP simulate more heatwave days than the other CP-RCM, which is consistent with the more marked warming TN and TX trends shown in Figure 3 and 4. Those differences could result from the influence of driving RCMs and GCMs. For instance, RegCM-ICTP shows a strong increase between HIST and LT periods (+42.9 and +42.2 heatwave days per year in rural and urban environments, respectively), probably in response to the warm signal of the HadGEM2-ES GCM (Collins et al., 2008). Figure 6a also displays interesting insights related to the different surface schemes used by CP-RCMs. As expected, without urban representation, CCLM-BTU shows similar increase trends for both urban and natural environments, with differences of less than or equal to 0.1 days per year in MT and LT, respectively. In contrast, other models show a larger average number of heatwave days per year in natural environments compared to urban areas, between +0.7 to +3.7 days per year for MT (except for

AROME-CNRM) and between +1.9 to +8.4 days per year for LT, highlighting a pronounced response of the natural environment to climate forcing. A similar finding was made in the single-model study of Michau et al., 2024 using the CP-RCM CNRM-AROME. Nevertheless, a comparison of the results of the different CP-RCMs does not reveal any typical responses depending on whether the model uses a slab or UCM approach. Finally, the impacts of climate change on urban and natural environments are more pronounced when considering the heatwave duration (Figure 6b). Several models show, in both median and extreme values, that heatwaves may last longer in rural than in urban areas by the end of the century.

3.3.1 Urban heat islands during heatwaves

In order to better understand the differences in behaviour between urban and natural areas, urban heat islands are here analyzed more specifically for heatwave periods, as done in Michau et al. (2024). Figure 7 shows the changes in UHIN and UHIX during heatwave days between the HIST period and the two future periods for the different models. Over the HIST period, the UHIX intensities calculated on heatwave days are slightly lower than those calculated previously on average over the summer (see JJA in Figure 5, left panel). On the other hand, the UHIN intensities are higher during heatwaves (in response to climatic conditions favouring and amplifying the nocturnal phenomenon) with variations between CP-RCM which are in agreement with those already noted for JJA.

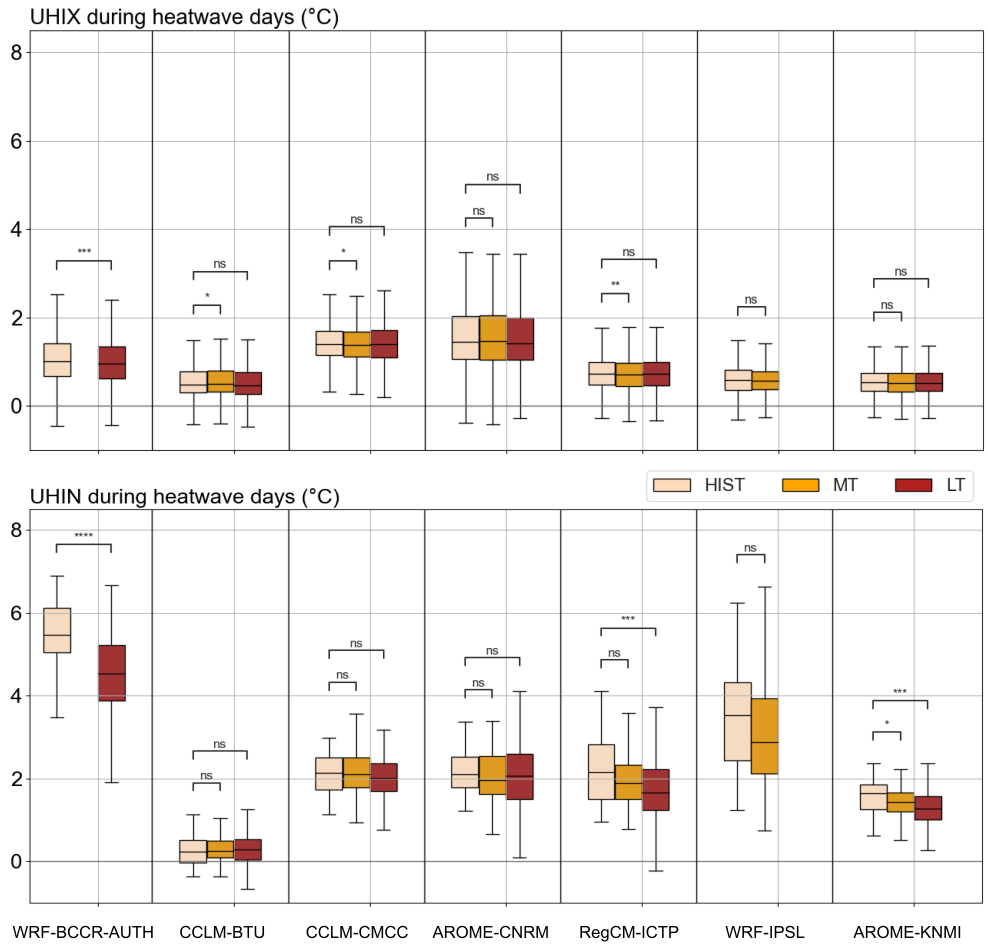

Figure 7. Changes in the daytime (top) and nighttime (bottom) UHI during heatwave days (in °C) between HIST (light orange), MT (orange) and LT (red) periods. Differences between distributions were assessed using the Mann-Whitney non-parametric test adapted for independent samples with hypotheses H0 (medians are equal) and H1 (medians are different). Symbols refer to the following significance thresholds: ***: 1e-4 $\leq$ p-value $\leq$ 1e-3, **: 1e-3 $\leq$ p-value $\leq$ 1e-2, *: 1e-2 $\leq$ p-value $\leq$ 0.05, ns (not significant): 0.05 $\leq$ p-value $\leq$ 1.

When comparing the different time periods, Figure 7 shows that among the five urbanized CP-RCMs that cover HIST and LT periods, three of them (WRF-BCCR-AUTH, RegCM-ICTP, AROME-KNMI) indicate a significant decrease in UHIN intensity during heatwave conditions. CCLM-CMCC shows a decrease in the median, but this is not statistically significant. As for AROME-CNRM, it shows no decrease, although this was the case in previous analyses by Michau et al. (2024), but over an extended future simulation period covering 2080-2099 and the northwestern domain (NW-3). This raises questions about the length of the analysis period needed to perform robust urban climate projection studies. It can be seen that the trends obtained on a seasonal scale (JJA in Figure 5) or during heatwaves are not necessarily in agreement. In Figure 5, only AROME-KNMI shows a significant downward trend in summer UHIN. In contrast, for the UHIX, the seasonal summer trends show a significant drop for three CP-RCMs, while there is very little signal for heatwave days.

4 Conclusions

A multi-model ensemble of simulations has been performed in the coordinated FPS Convection project. In total, seven CP-RCMs using urban climate module with different levels of sophistication were used for the present study over an historical period and at least one future period (mid- or long-term). Using this ensemble of simulations, this paper addressed several scientific questions related to the simulation of the urban climate and its evolution with climate change. Specifically, a first objective was to evaluate the ability of the CP-RCMs to simulate the urban climate, taking into account their characteristics, the modeling chain, the type of surface scheme that they used, and the presence or absence of a dedicated parameterization (urban module) to simulate the urban physical processes. A second objective was to assess the models' agreement on the projection of regional temperatures, urban climate, and heatwaves with climate change.

First, the analysis and comparison of CP-RCM results over the HIST period

showed that the CP-RCMs with an urban surface parameterization were able to represent the UHIs (daytime abd nighttime), including their typical seasonal variation. However, this comparison did not reveal any difference in performance between the CP-RCMs based on the simple slab approach and those incorporating an urban canopy model for representing urban areas (which should capture the nocturnal UHI better).

Based on the RCP8.5 GHG emission scenario, the multi-model ensemble projected a significant increase of mean annual temperature of around +3.7 °C in longterm period over the region of Paris, consistent with values reported in the literature over Metropolitan France using this GHG scenario (Soubeyroux et al., 2021). The study also highlighted that most CP-RCMs simulate a decrease of the UHI effect during daytime in JJA, similar to the results obtained by Hamdi et al. (2015) for Brussels, Belgium. This response could be attributed to a larger increase in temperatures in the natural environment surrounding the city, possibly due to a lack of precipitation and/or decrease of soil moisture, which could impact the cooling capacities of that environment with evaporation, as feature that had been raised in other studies (Mueller and Seneviratne, 2012; Oleson, 2012; Miralles et al., 2014; Le Roy et al., 2024). To confirm these results, it could be relevant to conduct an in-depth analysis of several meteorological parameters, including (1) precipitation, especially in the months preceding intense heat periods, (2) soil moisture content, and (3) latent and sensible heat fluxes. Finally, the analysis of the multimodel ensemble of projections indicated a strengthening of heatwaves for the end of the century period in terms of the number of heatwave days and duration, with a rather good agreement between the models' projections.

This first study of urban effects in a multi-model configuration is very promising. Nevertheless, some limitations regarding the configuration of the simulations or access to data could be highlighted. The ensemble of models used here is a bit too small and experiments too short-term (10 years) to carry out a robust sensitivity study on the variability of CP-RCM's performance and their projection of heatwaves and UHIs. This highlights the importance to define

a dedicated experimental protocol for urban climate in the future coordinated projects such as the FPS URB-RCC. This initiative aims to better understand the contribution of urban parameterizations and the level of sophistication needed to simulate more realistically the urban climate. For that end, the current experiment protocol should be reconsidered to facilitate intercomparison studies, providing more detailed information on models and surface databases. The original methodology developed and presented here, particularly for processing surface data and defining urban and natural masks, could be useful for future studies focusing on the simulation of the UHI with CP-RCMs.

References

Adinolfi, M., Raffa, M., Reder, A., & Mercogliano, P. (2023). Investigation on potential and limitations of era5 reanalysis downscaled on italy by a convection-permitting model. *Climate dynamics*. https://doi.org/10.1007/s00382-023-06803-w

Ban, N., Caillaud, C., Coppola, E., Pichelli, E., Sobolowski, S., Adinolfi, M., Ahrens, B., Alias, A., Anders, I., Bastin, S., Belušić, D., Berthou, S., Brisson, E., Cardoso, R. M., Chan, S. C., Christensen, O. B., Fernández, J., Fita, L., Frisius, T., ... Zander, M. J. (2021). The first multi-model ensemble of regional climate simulations at kilometer-scale resolution, part i: Evaluation of precipitation. *Climate Dynamics*, *57*(1-2), 275–302. https://doi.org/10.1007/s00382-021-05708-w

Bartholomé, E., & Belward, A. S. (2005). GLC2000: A new approach to global land cover mapping from earth observation data. *International Journal of Remote Sensing*, *26*(9), 1959–1977. https://doi.org/10.1080/01431160412331291297

Belušić, D., de Vries, H., Dobler, A., Landgren, O., Lind, P., Lindstedt, D., Pedersen, R. A., Sánchez-Perrino, J. C., Toivonen, E., van Ulft, B., Wang, F., Andrae, U., Batrak, Y., Kjellström, E., Lenderink, G., Nikulin, G., Pietikäinen, J.-P., Rodríguez-Camino, E., Samuelsson, P., ... Wu, M. (2020). HCLIM38: A flexible regional climate model applicable for different climate zones from coarse to convection-permitting scales. *Geoscientific Model Development*, *13*(3), 1311–1333. https://doi.org/10.5194/gmd-13-1311-2020

Bentsen, M., Bethke, I., Debernard, J. B., Iversen, T., Kirkevåg, A., Seland, Ø., Drange, H., Roelandt, C., Seierstad, I. A., Hoose, C., & Kristjánsson, J. E. (2013). The norwegian earth system model, NorESM1-m – part 1: Description and basic evaluation of the physical climate. *Geoscientific Model Development*, *6*(3), 687–720. https://doi.org/10.5194/gmd-6-687-2013

Besson, F., Dubuisson, B., Etchevers, P., Gibelin, A.-L., Lassegues, P., Schneider, M., & Vincendon, B. (2019). Climate monitoring and heat and cold waves detection over france using a new spatialization of daily temperature extremes from 1947 to present. *Advances in Science and Research*, *16*, 149–156. https://doi.org/10.5194/asr-16-149-2019

Boone, A., Calvet, J.-C., & Noilhan, J. (1999). Inclusion of a third soil layer in a land surface scheme using the force–restore method. *Journal of Applied Meteorology*, *38*(11), 1611–1630. https://doi.org/10.1175/1520-0450(1999)038⟨1611:ioatsl⟩2.0.co;2

Caillaud, C., Somot, S., Alias, A., Bernard-Bouissières, I., Fumière, Q., Laurantin, O., Seity, Y., & Ducrocq, V. (2021). Modelling mediterranean heavy precipitation events at climate scale: An object-oriented evaluation of the CNRM-AROME convection-permitting regional climate model. *Climate Dynamics*, *56*(5-6), 1717–1752. https://doi.org/10.1007/s00382-020-05558-y

Champeaux, J.-L., Masson, V., & Chauvin, F. (2005). ECOCLIMAP: A global database of land surface parameters at 1 km resolution. *Meteorological Applications*, *12*(1), 29–32. https://doi.org/10.1017/s1350482705001519

Collins, W. J., Bellouin, N., Doutriaux-Boucher, M., Gedney, N., Hinton, T., andS. Liddicoat, C. D. J., Martin, G., O'Connor, F., Rae, J., Senior, C., Totterdell, I., & Woodward., S. (2008). *Hadley centre technical note 74: Evaluation of the hadgem2 model.* (tech. rep.). Met Office Hadley Centre.

Coppola, E., Sobolowski, S., Pichelli, E., Raffaele, F., Ahrens, B., Anders, I., Ban, N., Bastin, S., Belda, M., Belusic, D., Caldas-Alvarez, A., M, C. R., Davolio, S., Dobler, A., Fernandez, J., Fita, L., Fumiere, Q., Giorgi, F., Goergen, K., ... Warrach-Sagi, K. (2020). A first-of-its-kind multi-model convection permitting ensemble for investigating convective phenomena over europe and the mediterranean. *Climate dynamics*. https://doi.org/10.1007/s00382-018-4521-8

Coppola, E., Stocchi, P., Pichelli, E., Alavez, J. A. T., Glazer, R., Giuliani, G., Sante, F. D., Nogherotto, R., & Giorgi, F. (2021). Non-hydrostatic

RegCM4 (RegCM4-NH): Model description and case studies over multiple domains. *Geosci. Model Dev.* https://doi.org/10.5194/gmd-2020-435

Decharme, B., Boone, A., Delire, C., & Noilhan, J. (2011). Local evaluation of the interaction between soil biosphere atmosphere soil multilayer diffusion scheme using four pedotransfer functions. *Journal of Geophysical Research*, *116*(D20). https://doi.org/10.1029/2011jd016002

Decharme, B., Brun, E., Boone, A., Delire, C., Moigne, P. L., & Morin, S. (2016). Impacts of snow and organic soils parameterization on northern eurasian soil temperature profiles simulated by the ISBA land surface model. *The Cryosphere*, *10*(2), 853–877. https://doi.org/10.5194/tc-10-853-2016

de Vries, H., Lenderink, G., van Meijgaard, E., van Ulft, B., & de Rooy, W. (2024). Western europe's extreme july 2019 heatwave in a warmer world. *Environmental Research: Climate*. https://doi.org/10.1088/2752-5295/ad519f

Dobson, J. E., Brlght, E. A., Coleman, P. R., Durfee, R. C., & Worley, B. A. (2000). Landscan:a global population database forestimating populations at risk. *Photogrammetric Engineering & Remote Sensing*, *66*(7).

Doms, G., Forstner, J., Heise, E., Herzog, H. J., Raschendorfer, M., Schrodin, R., Reinhardt, T., & Vogel, G. (2005). *A Description of theNonhydrostatic Regional Model LM. Part II: Physical Parameterization* (tech. rep.). Consortium for Small-Scale Modelling.

Douville, H., Royer, J.-F., & Mahfouf, J. F. (1995). A new snow parameterization for the météo-france climate model. *Climate Dynamics*, *12*(1), 21–35. https://doi.org/10.1007/bf00208760

Dufresne, J.-L., Foujols, M.-A., Denvil, S., Caubel, A., Marti, O., Aumont, O., Balkanski, Y., Bekki, S., Bellenger, H., Benshila, R., Bony, S., Bopp, L., Braconnot, P., Brockmann, P., Cadule, P., Cheruy, F., Codron, F., Cozic, A., Cugnet, D., ... Vuichard, N. (2013). Climate change projections using the IPSL-CM5 earth system model: From CMIP3 to CMIP5. *Climate Dynamics*, *40*(9-10), 2123–2165. https://doi.org/10.1007/s00382-012-1636-1

Ek, M., Mitchell, K., Lin, Y., Rogers, E., Grunmann, P., Koren, V., Gayno, G., & Tarpley, J. (2003). Implementation of noah land surface model advances in the national centers for environmental prediction operational mesoscale eta model. *J. Geophys. Res.*

Faroux, S., Tchuenté, A. T. K., Roujean, J. L., Masson, V., Martin, E., & Moigne, P. L. (2013). ECOCLIMAP-II/europe: A twofold database of ecosystems and surface parameters at 1 km resolution based on satellite information for use in land surface, meteorological and climate models. *Geoscientific Model Development*, *6*(2), 563–582. https://doi.org/10.5194/gmd-6-563-2013

Fosser, G., Gaetani, M., Kendon, E. J., Adinolfi, M., Ban, N., Belušić, D., Caillaud, C., Careto, J. A. M., Coppola, E., Demory, M.-E., de Vries, H., Dobler, A., Feldmann, H., Goergen, K., Lenderink, G., Pichelli, E., Schär, C., Soares, P. M. M., Somot, S., & Tölle, M. H. (2024). Convection-permitting climate models offer more certain extreme rainfall projections. *Climate and Atmospheric Science*. https://doi.org/10.1038/s41612-024-00600-w

García-Nieto, A. P., Geijzendorffer, I. R., Baró, F., Roche, P. K., Bondeau, A., & Cramer, W. (2018). Impacts of urbanization around mediterranean cities: Changes in ecosystem service supply. *Ecological Indicators*, *91*, 589–606. https://doi.org/10.1016/j.ecolind.2018.03.082

Giorgi, F., Coppola, E., Solmon, F., Mariotti, L., Sylla, M., Bi, X., Elguindi, N., Diro, G., Nair, V., Giuliani, G., Turuncoglu, U., Cozzini, S., Güttler, I., O'Brien, T. A., Tawfik, A., Shalaby, A., Zakey, A., Steiner, A., Stordal, F., ... Brankovic, C. (2012). RegCM4: Model description and preliminary tests over multiple CORDEX domains. *Climate Research*, *52*, 7–29. https://doi.org/10.3354/cr01018

Hamdi, R., Giot, O., Troch, R. D., Deckmyn, A., & Termonia, P. (2015). Future climate of brussels and paris for the 2050s under the a1b scenario. *Urban Climate*, *12*, 160–182. https://doi.org/10.1016/j.uclim.2015.03.003

Hamdi, R., & Masson, V. (2008). Inclusion of a drag approach in the town energy balance (TEB) scheme: Offline 1d evaluation in a street canyon.

Journal of Applied Meteorology and Climatology, *47*(10), 2627–2644. https://doi.org/10.1175/2008jamc1865.1

Hazeleger, W., Wang, X., Severijns, C., Ştefănescu, S., Bintanja, R., Sterl, A., Wyser, K., Semmler, T., Yang, S., van den Hurk, B., van Noije, T., van der Linden, E., & van der Wiel, K. (2011). EC-earth v2.2: Description and validation of a new seamless earth system prediction model. *Climate Dynamics*, *39*(11), 2611–2629. https://doi.org/10.1007/s00382-011-1228-5

IPCC. (2021). Climate Change 2021: The physical science basis. Contribution of working group I to the Sixth Assessment Report of the Intergovernmental Panel on Climate Change (V. Masson-Delmotte, P. Zhai, A. Pirani, S. L. Connors, C. Péan, S. Berger, N. Caud, Y. Chen, L. Goldfarb, M. I. Gomis, M. Huang, K. Leitzell, E. Lonnoy, J. B. R. Matthews, T. K. Maycock, T. Waterfield, O. Yelekçi, R. Yu, & B. Zhou, Eds.). https://doi.org/10.1017/9781009157896

Jones, C. D., Hughes, J. K., Bellouin, N., Hardiman, S. C., Jones, G. S., Knight, J., Liddicoat, S., O'Connor, F. M., Andres, R. J., Bell, C., Boo, K.-O., Bozzo, A., Butchart, N., Cadule, P., Corbin, K. D., Doutriaux-Boucher, M., Friedlingstein, P., Gornall, J., Gray, L., ... Zerroukat, M. (2011). The HadGEM2-ES implementation of CMIP5 centennial simulations. *Geoscientific Model Development*, *4*(3), 543–570. https://doi.org/10.5194/gmd-4-543-2011

Kendon, E. J., Prein, A. F., Senior, C. A., & Stirling, A. (2021). Challenges and outlook for convection-permitting climate modelling. *379*(2195), 20190547. https://doi.org/10.1098/rsta.2019.0547

Keuler, K., Radtke, K., Kotlarski, S., & Lüthi, D. (2016). Regional climate change over europe in COSMO-CLM: Influence of emission scenario and driving global model. *Meteorologische Zeitschrift*, *25*(2), 121–136. https://doi.org/10.1127/metz/2016/0662

Knist, S., Goergen, K., Buonomo, E., Christensen, O. B., Colette, A., Cardoso, R. M., Fealy, R., Fernández, J., García-Díez, M., Jacob, D., Kartsios, S., Katragkou, E., Keuler, K., Mayer, S., van Meijgaard, E., Nikulin, G.,

Soares, P. M. M., Sobolowski, S., Szepszo, G., ... Simmer, C. (2017). Land-atmosphere coupling in EURO-CORDEX evaluation experiments. *Journal of Geophysical Research: Atmospheres*, *122*(1), 79–103. https://doi.org/10.1002/2016jd025476

Kusaka, H., Kondo, H., Kikegawa, Y., & Kimura, F. (2001). A simple single-layer urban canopy model for atmospheric models: Comparison with multi-layer and slab models. *Boundary-Layer Meteorology*, *101*(3), 329–358. https://doi.org/10.1023/a:1019207923078

Laaidi, K., Zeghnoun, A., Dousset, B., Bretin, P., Vandentorren, S., Giraudet, E., & Beaudeau, P. (2012). The impact of heat islands on mortality in paris during the august 2003 heat wave. *Environmental Health Perspectives*, *120*(2), 254–259. https://doi.org/10.1289/ehp.1103532

Langendijk, G. S., Halenka, T., Hoffmann, P., Adinolfi, M., Aldama Campino, A., Asselin, O., Bastin, S., Bechtel, B., Belda, M., Bushenkova, A., Campanale, A., Chun, K. P., Constantinidou, K., Coppola, E., Demuzere, M., Doan, Q.-V., Evans, J. P., Feldmann, H., Fernandez, J., ... Yuan, J. (2024). Towards better understanding the urban environment and its interactions with regional climate change -the wcrp cordex flagship pilot study urb-rcc. https://doi.org/10.2139/ssrn.4846089

Le Roy, B., Lemonsu, A., Schoetter, R., & Machado, T. (2024). Study of the future evolution of the urban climate of paris by statistical-dynamical downscaling of the euro-cordex ensemble. *J. Appl. Meteor. Climatol.* https://doi.org/10.1175/JAMC-D-23-0145.1

Lemonsu, A., Caillaud, C., Alias, A., Riette, S., Seity, Y., Roy, B. L., Michau, Y., & Lucas-Picher, P. (2023). What added value of CNRM-AROME convection-permitting regional climate model compared to CNRM-ALADIN regional climate model for urban climate studies ? evaluation over paris area (france). *Climate Dynamics*. https://doi.org/10.1007/s00382-022-06647-w

Lucas-Picher, P., Brisson, E., Caillaud, C., Alias, A., Nabat, P., Lemonsu, A., Poncet, N., Hernandez, V. E. C., Michau, Y., Doury, A., Monteiro, D., & Somot, S. (2023). Evaluation of the convection-permitting regional

climate model CNRM-AROME41t1 over northwestern europe. *Climate Dynamics*. https://doi.org/10.1007/s00382-022-06637-y

Masson, V. (2000). A physically-based scheme for the urban energy budget in atmospheric models. *Boundary-Layer Meteorology*, *94*(3), 357–397. https://doi.org/10.1023/a:1002463829265

Masson, V., Moigne, P. L., Martin, E., Faroux, S., Alias, A., Alkama, R., Belamari, S., Barbu, A., Boone, A., Bouyssel, F., Brousseau, P., Brun, E., Calvet, J.-C., Carrer, D., Decharme, B., Delire, C., Donier, S., Essaouini, K., Gibelin, A.-L., ... Voldoire, A. (2013). The SURFEXv7.2 land and ocean surface platform for coupled or offline simulation of earth surface variables and fluxes. *Geoscientific Model Development*, *6*(4), 929–960. https://doi.org/10.5194/gmd-6-929-2013

Michau, Y., Lemonsu, A., Lucas-Picher, P., Schneider, M., & Caillaud, C. (2024). On the future evolution of heatwaves in french cities and associated rural areas: Insights from a convection-permitting model. *Urban Climate*. https://doi.org/10.1016/j.uclim.2024.101920

Miralles, D. G., Teuling, A. J., van Heerwaarden, C. C., & de Arellano, J. V.-G. (2014). Mega-heatwave temperatures due to combined soil desiccation and atmospheric heat accumulation. *Nature Geoscience*, *7*(5), 345–349. https://doi.org/10.1038/ngeo2141

Molina, M. O., Careto, J. M., Gutiérrez, C., Sánchez, E., Goergen, K., Sobolowski, S., Coppola, E., Pichelli, E., Ban, N., Belusić, D., Short, C., Caillaud, C., Dobler, A., Hodnebrog, Ø., Kartsios, S., Lenderink, G., de Vries, H., Göktürk, O., Milovac, J., ... Soares, P. M. M. (2024). The added value of simulated near-surface wind speed over the alps from a km-scale multimodel ensemble. *Climate dynamics*. https://doi.org/10.1007/s00382-024-07257-4

Molina, M. O., Sánchez, E., & Gutiérrez, C. (2020). Future heat waves over the mediterranean from an euro-CORDEX regional climate model ensemble. *Scientific Reports*, *10*(1). https://doi.org/10.1038/s41598-020-65663-0

Mueller, B., & Seneviratne, S. I. (2012). Hot days induced by precipitation deficits at the global scale. *Proceedings of the National Academy of Sciences*, *109*(31), 12398–12403. https://doi.org/10.1073/pnas.1204330109

Nabat, P., Somot, S., Cassou, C., Mallet, M., Michou, M., Bouniol, D., Decharme, B., Drugé, T., Roehrig, R., & Saint-Martin, D. (2020). Modulation of radiative aerosols effects by atmospheric circulation over the euro-mediterranean region. *Atmospheric Chemistry and Physics*, *20*(14), 8315–8349. https://doi.org/10.5194/acp-20-8315-2020

Niu, G.-Y., Yang, Z.-L., Mitchell, K. E., Chen, F., Ek, M. B., Barlage, M., Kumar, A., Manning, K., Niyogi, D., Rosero, E., Tewari, M., & Xia, Y. (2011). The community noah land surface model with multiparameterization options (noah-MP): 1. model description and evaluation with local-scale measurements. *Journal of Geophysical Research*, *116*(D12). https://doi.org/10.1029/2010jd015139

Oke, T. R., Mills, G., Christen, A., & Voogt, J. A. (2017). *Urban climates*. Cambridge University Press. https://doi.org/10.1017/9781139016476

Oleson, K. (2012). Contrasts between urban and rural climate in CCSM4 CMIP5 climate change scenarios. *Journal of Climate*, *25*(5), 1390–1412. https://doi.org/10.1175/jcli-d-11-00098.1

Oleson, K., Bonan, G., Feddema, J., Vertenstein, M., & Kluzek, E. (2010). *Technical description of an urban parameterization for the community land model (clmu)* (tech. rep.). NCAR Earth System Laboratory. UCAR/NCAR. https://doi.org/10.5065/D6K35RM9

Oleson, K. W., & Lawrence, D. M. (2013). *Technical description of version 4.5 of the community land model (clm)* (tech. rep.). NCAR Earth System Laboratory.

Ouzeau, G., Soubeyroux, J.-M., Schneider, M., Vautard, R., & Planton, S. (2016). Heat waves analysis over france in present and future climate: Application of a new method on the EURO-CORDEX ensemble. *Climate Services*, *4*, 1–12. https://doi.org/10.1016/j.cliser.2016.09.002

Perkins, S. E. (2015). A review on the scientific understanding of heatwaves—their measurement, driving mechanisms, and changes at the global scale. *Atmo-*

spheric Research, *164-165*, 242–267. https://doi.org/10.1016/j.atmosres.2015.05.014

Pichelli, E., Coppola, E., Sobolowski, S., Ban, N., Giorgi, F., Stocchi, P., Alias, A., Belušić, D., Berthou, S., Caillaud, C., Cardoso, R. M., Chan, S., Christensen, O. B., Dobler, A., de Vries, H., Goergen, K., Kendon, E. J., Keuler, K., Lenderink, G., ... Vergara-Temprado, J. (2021). The first multi-model ensemble of regional climate simulations at kilometer-scale resolution part 2: Historical and future simulations of precipitation. *Climate Dynamics*, *56*(11-12), 3581–3602. https://doi.org/10.1007/s00382-021-05657-4

Robine, J. M., Cheung, S. L. K., Roy, S. L., Oyen, H. V., Griffiths, C., Michel, J.-P., & Herrmann, F. R. (2008). Death toll exceeded 70.000 in europe during the summer of 2003. *Comptes Rendus Biologies*, *331*(2), 171–178. https://doi.org/10.1016/j.crvi.2007.12.001

Rockel, B., Will, A., & Hense, A. (2008). The regional climate model COSMO-CLM (CCLM). *17*(4), 347–348. https://doi.org/10.1127/0941-2948/2008/0309

Sangelantoni, L., Sobolowski, S., Lorenz, T., Hodnebrog, Ø., Cardoso, R. M., Soares, P. M. M., Ferretti, R., Lavín-Gullón, A., Fernandez, J., Goergen, K., Milovac, J., Katragkou, E., Kartsios, S., Coppola, E., Pichelli, E., Adinolfi, M., Mercogliano, P., Berthou, S., de Vries, H., ... Bastin, S. (2023). Investigating the representation of heatwaves from an ensemble of km-scale regional climate simulations within CORDEX-FPS convection. *Climate Dynamics*. https://doi.org/10.1007/s00382-023-06769-9

Schrodin, R., & Heise, E. (2001). The multi-layer-version of the dwdsoil model terra/lm, consortium for small-scale modelling(cosmo) tech. rep., 2, 16 pp.

Skamarock, W., Klemp, J., Dudhia, J., Gill, D., Barker, D., Wang, W., Huang, X.-Y., & Duda, M. (2008). *A description of the advanced research wrf version 3* (tech. rep.). UCAR/NCAR. https://doi.org/10.5065/D68S4MVH

Skamarock, W. C., & Klemp, J. B. (2008). A time-split nonhydrostatic atmospheric model for weather research and forecasting applications. *Journal*

of Computational Physics, *227*(7), 3465–3485. https://doi.org/10.1016/j.jcp.2007.01.037

Soubeyroux, J.-M., Bernus, S., Corre, L., Drouin, A., Dubuisson, B., Etchevers, P., Gouget, V., Josse, P., Kerdoncuff, M., Samacoits, R., & Tocquer, F. (2021). Les nouvelles projections climatiques de référence drias 2020 pour la métropole. *Climate Dynamics*.

van Meijgaard, E., van Ulft, L. H., Lenderink, G., de Roode, S. R., Wipfler, L., Boers, R., & Timmermans, R. M. A. (2012). Refinement and application of a regional atmospheric model for climate scenario calculations of western europe. *Climate changes Spatial Planning*. https://library.wur.nl/WebQuery/wurpubs/fulltext/312258

van Meijgaard, E., van Ulft, L. H., van de Berg W.J., van den Hurk B.J.J.M., Lenderink, G., & Siebesma, A. P. (2008). The knmi regional atmospheric climate model racmo version 2.1. knmi technical report.

Vautard, R., Kadygrov, N., Iles, C., Boberg, F., Buonomo, E., Bülow, K., Coppola, E., Corre, L., van Meijgaard, E., Nogherotto, R., Sandstad, M., Schwingshackl, C., Somot, S., Aalbers, E., Christensen, O. B., Ciarlo, J. M., Demory, M.-E., Giorgi, F., Jacob, D., … Wulfmeyer, V. (2021). Evaluation of the large euro-cordex regional climate model ensemble. *Journal of Geophysical Research: Atmospheres*. https://doi.org/10.1029/2019JD032344

Voldoire, A., Sanchez-Gomez, E., y Mélia, D. S., Decharme, B., Cassou, C., Sénési, S., Valcke, S., Beau, I., Alias, A., Chevallier, M., Déqué, M., Deshayes, J., Douville, H., Fernandez, E., Madec, G., Maisonnave, E., Moine, M.-P., Planton, S., Saint-Martin, D., … Chauvin, F. (2012). The CNRM-CM5.1 global climate model: Description and basic evaluation. *Climate Dynamics*, *40*(9-10), 2091–2121. https://doi.org/10.1007/s00382-011-1259-y

Wouters, H., Demuzere, M., Ridder, K. D., & van Lipzig, N. P. M. (2015). The impact of impervious water-storage parametrization on urban climate modelling. *Urban Climate*, *11*, 24–50. https://doi.org/10.1016/j.uclim.2014.11.005

Yang, W., Tan, B., Huang, D., Rautiainen, M., Shabanov, N., Wang, Y., Privette, J., Huemmrich, K., Fensholt, R., Sandholt, I., Weiss, M., Ahl, D., Gower,

S., Nemani, R., Knyazikhin, Y., & Myneni, R. B. (2006). MODIS leaf area index products: From validation to algorithm improvement. *IEEE Transactions on Geoscience and Remote Sensing*, *44*(7), 1885–1898. https://doi.org/10.1109/tgrs.2006.871215

Acknowledgments

The authors thank the WCRP-CORDEX-FPS on high-resolution convective phenomena over Europe and the Mediterranean (FPSCONV-ALP-3) and on urban environments and regional climate change (FPS-URB RCC). The author would like to thank Graziano Giuliani from the International Centre for Theoretical Physic (ICTP), Ozan Mert Göktürk and Stefan Sobolowski, both from the NORCE Norwegian Research Centre AS, and Bert van Ulft from the Royal Netherlands Meteorological Institute (KNMI), for their advice in reviewing the article. We are also grateful for the research data exchange infrastructure and services provided by the Jülich Supercomputing Center, Germany, as part of the Helmholtz Data Federation initiative.

Statements and declarations

Funding

This research is a contribution to the project KM-Impacts funded by the Make Our Planet Great Again initiative that is supported by the French National Research Agency under the future investment programme ANR-18-MPGA-0005.

Competing interests

The authors declare that they have no known competing financial interests or personal relationships that could have appeared to influence the work reported in this paper.

Data availability

The datasets generated during and/or analyzed during the current study are available from the corresponding author on reasonable request.